CHINESE OPTICS LETTERS

Vol. 19, No. 6 | June 2021

Surface lattice resonances in dielectric metasurfaces for enhanced light-matter interaction [Invited]

Yuechen Jia (贾曰辰)[1*], Yingying Ren (任莹莹)[2], Xingjuan Zhao (赵兴娟)[1], and Feng Chen (陈 峰)[1**]

[1] School of Physics, State Key Laboratory of Crystal Materials, Shandong University, Jinan 250100, China

[2] Shandong Provincial Engineering and Technical Center of Light Manipulations & Shandong Provincial Key Laboratory of Optics and Photonic Device, School of Physics and Electronics, Shandong Normal University, Jinan 250014, China

*Corresponding author: yuechen.jia@sdu.edu.cn

**Corresponding author: drfchen@sdu.edu.cn

Received March 19, 2021 | Accepted April 30, 2021 | Posted Online May 31, 2021

Lithium niobate ($LiNbO_3$) is a versatile crystalline material for various photonic applications. With the recent advances in $LiNbO_3$-on-insulator (LNOI) thin film technology, $LiNbO_3$ has been regarded as one of the most promising platforms for multifunctional integrated photonics. In this work, we present the field enhancement due to collective resonances in arrayed $LiNbO_3$ nanoantennas. These resonances arise from the enhanced radiative coupling of localized Mie resonances in the individual nanoparticles and Rayleigh anomalies due to in-plane diffraction orders of the lattice. We describe the pronounced differences in field enhancement and field distributions for electric and magnetic dipoles, offering valuable information for the design and optimization of high-quality-factor optical metasurfaces based on $LiNbO_3$.

Keywords: integrated optics; nanophotonics; lithium niobate; Mie theory.

DOI: 10.3788/COL202119.060013

1. Introduction

Using nanostructures/nanoparticles with diverse morphology for light field manipulation at the nanoscale has been one of the central topics in nanophotonics over the past years[1,2]. With proper designs of single nanoparticles or arrayed nanoantennas, it is possible to nicely tune optical field confinement and scattering, leading to local field enhancement, increased light–matter interaction, enhanced nonlinear optical effects, as well as high sensitivity to small perturbations. Applications of this optical enhancement effect span from bio-sensing and imaging to optoelectronic devices[3–5]. Particularly, metasurfaces, as the two-dimensional counterparts of metamaterials, are of great promise for efficient nonlinear optical frequency conversion compared to standard nonlinear optical materials due to the relaxation or even complete overcoming of the phase-matching constrains[6–8]. In this regard, metallic nanoparticles/nanoantennas, which are able to provide both strong optical field enhancement and good optical confinement, have been intensively investigated[9–12]. However, intrinsic to metals are Ohmic losses due to free-electron scattering, limiting the efficiency of plasmonic nanophotonic devices for applications in, for example, nonlinear optics. In contrast, high-refractive-index dielectric materials supporting Mie resonances provide very low optical losses at optical frequencies[6,13–16]. Moreover, apart from high tolerance of much higher pump intensities, dielectric nanostructures are able to exhibit both electric and magnetic resonances, which gives the freedom to design various all-dielectric nanostructures with resonances at a desirable range of wavelength[6]. These features make dielectric metasurfaces a promising route for obtaining enhanced nonlinear optical frequency conversion efficiency.

Among all of the dielectric materials, lithium niobate ($LiNbO_3$) is an ideal candidate for the existing nonlinear optical applications over its wideband optical transparency window (wavelength range from 400 nm to 5 μm, with an OH-absorption peak at 2.87 μm)[17–19]. In addition, $LiNbO_3$ possesses excellent electro-optic (EO), acousto-optic (AO), piezoelectric, and pyroelectric properties, rendering it a unique platform for various applications. Since $LiNbO_3$ is notoriously difficult to etch, its practical application in integrated photonics and nanophotonics has been limited over a long period of time. With the tremendous development in $LiNbO_3$-on-insulator (LNOI) thin film technology and surface nanostructuring techniques, $LiNbO_3$-based on-chip photonic devices such as waveguides, microcavities, and even metasurfaces have been recently demonstrated[20–33]. In contrast to high-refractive-index semiconductor-based metasurfaces (e.g., Si metasurfaces), however, $LiNbO_3$ metasurfaces are not able to support strong Mie resonances due to the relatively low refractive index contrast between active $LiNbO_3$ ($n_{o,\mathrm{LN}} \approx 2.21$ and $n_{e,\mathrm{LN}} \approx 2.14$ at 1.55 μm) and

supporting substrate (generally SiO_2 with a refractive index of $n_{SiO_2} \approx 1.44$ at 1.55 μm).

On a different front, arrayed plasmonic nanoantennas supporting collective resonances have received significant attention due to their remarkably high quality factors as well as high field enhancements over large volumes[34–36]. These collective resonances originate from the occurrence of electromagnetic coupling between periodically arrayed nanoscatterers due to diffractive effects. In particular, the diffraction orders in the plane of the array, known as Rayleigh anomalies (RAs), are able to enhance the radiative coupling[37–39]. Correspondingly, the collective resonances located close to the RAs of the array are the so-called surface lattice resonances (SLRs), which can be described as a Fano-type process involving a broad resonance (localized surface plasmon resonances) and a discrete mode associated with the scattering that occurred in the plane of the array at different-order RA positions. It has been proved that lattice modes offer an enhanced scattering and thus a high quality factor of collective resonances in metallic arrays[37–39].

In this work, based on the LNOI thin film platform, we present a detailed theoretical analysis of collective resonances of SLRs and Mie resonances, including electric dipole (ED) and magnetic dipole (MD), in arrays of $LiNbO_3$ nanoparticles using COMSOL simulations. Despite the hybridized scattering effects for ED and MD modes being very different, both illustrate strong electromagnetic field confinements and enhancements based on near-field simulations, respectively. In particular, the impact from nanoparticle side-wall angles on the resulting field enhancements is also studied.

2. Theoretical Analysis

Theoretical analyses of a single $LiNbO_3$ nanoparticle and an arrayed $LiNbO_3$ nanoantenna on a SiO_2 substrate are performed using a commercial finite element method (FEM)-based software: COMSOL Multiphysics and Optics Module. All of the nanoparticles sharp edges are rounded with a radius of curvature of 77 nm to better resemble the fabricated nanostructures in practice. The refractive indices of active $LiNbO_3$ (z-cut, with n_o along the x and y orientations and n_e along the z orientation) thin film layer and SiO_2 substrate are taken from Refs. [40,41]. The response of an infinite array of $LiNbO_3$ nanoantennas is obtained by imposing appropriate periodic boundary conditions in the array plane. Our simulation focuses on the design of monolithic metasurfaces in a z-cut LNOI thin film because it is potentially easier for nanostructuring. Two perfectly matched layers (PMLs) are instead set as boundary conditions at the top (air) and the bottom (SiO_2 substrate) of the calculation domain, to avoid spurious reflections. In the solver, the Floquet periodic boundary conditions are imposed on four sides of the unit cell to simulate the infinite two-dimensional array of nanoantennas. For the input illumination conditions in the simulation, a linearly polarized (x-polarized) plane wave propagating along the normal direction (i.e., z axis) is employed. The injection angle was set to zero to simulate a normally incident wave. To calculate the maximum electric field enhancement in the $LiNbO_3$ nanoparticle, a domain probe is placed inside the nanoparticle in the simulation.

3. Results and Discussion

3.1. Single $LiNbO_3$ nanoparticle

The optical resonances (Mie resonances) supported by individual $LiNbO_3$ nanoparticles in air are studied. The nanoparticles have a truncated square pyramid (as illustrated in Fig. 1) with rounded edges and are located on a SiO_2 substrate with air superstrate. The height $h = 950$ nm, the length (equal to the width) $d = 800$ nm, and the side-wall angle $\theta = 5°$ (the nanoparticle dimension has been optimized in order to achieve high field enhancement around 1.5 μm) are selected so that both electric and magnetic modes can be supported, particularly the lowest-order modes, i.e., the ED and MD (as shown in Fig. 2) according to the Mie theory. The resonant ED modes arise from the displacement current along the incident light polarization (x-polarized). The resonant MD moments originate from the coupling of incident light to the circular displacement current of the electric field as a result of field penetration and phase retardation inside nanoparticles. Therefore, the MD resonance appears when the wavelength inside nanoparticles is comparable to its spatial dimension, while its height is sufficient for the formation of the displacement current loop. The resonance shift and enhancement of both ED and MD in the case of arrayed nanoantennas are the main research objects in this work. In particular, the side-wall angle has significant impacts on the optical confinement and field enhancement in arrayed nanoantennas, which will be discussed in the following section.

The scattering cross sections and the corresponding electric field enhancements (at wavelengths from 1400 nm to 2400 nm) of a single on-chip $LiNbO_3$ nanoparticle (with SiO_2 substrate and air superstrate according to the commercially available LNOI chip) are calculated, as shown in Fig. 2(a). To identify the nature of the ED and MD resonances at 1690 nm and 2100 nm, respectively, the spatial distributions of the electric and magnetic field intensity enhancements relative to the

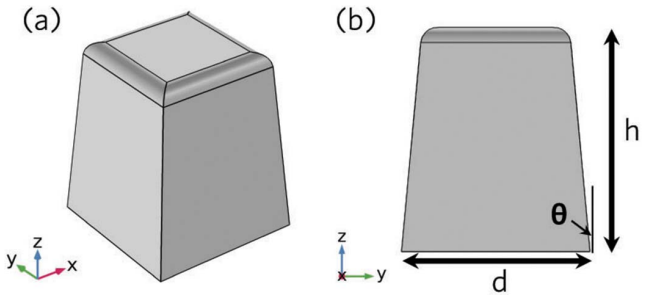

Fig. 1. (a) Schematic representation of a single $LiNbO_3$ nanoparticle used in this work. (b) Side profile of the nanoparticle with a height of h, a length and width of d, and a side-wall angle of θ. The x, y, and z axis orientations represent the $LiNbO_3$ crystalline axes.

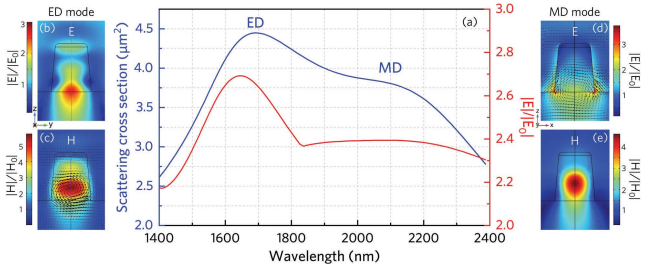

Fig. 2. (a) Simulated scattering cross section and electric field enhancement of an on-chip $LiNbO_3$ nanoparticle ($d = 800$ nm, $h = 960$ nm, $\theta = 5°$) with a SiO_2 substrate and air superstrate. The spatial distributions of the normalized (b), (d) electric field intensity and (c), (e) magnetic field intensity for the (b), (c) ED and the (d), (e) MD resonances. The color scales represent the field intensity, and the black arrows represent the real part of the vectorial (c) magnetic and (d) electric field projected in the (c) *yz* and (d) *xz* plane, respectively.

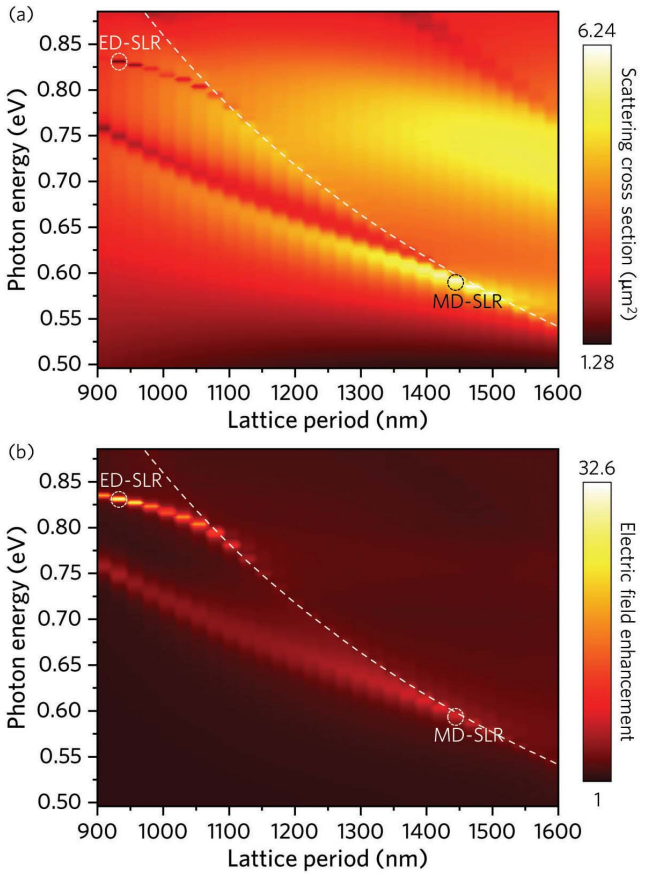

Fig. 3. COMSOL simulations of (a) scattering cross section and (b) electric field enhancement of arrayed $LiNbO_3$ nanoantennas with lattice period from 900 nm to 1600 nm. The maximum electric field enhancement positions for ED and MD modes are marked in the figures, labeled as ED-SLR and MD-SLR, respectively.

incident field intensity are investigated at the resonant frequencies [see Figs. 2(b)–2(e)]. The field circulations in Figs. 2(c) and 2(d) confirm the formation of the ED and MD resonances[42]. However, using the standard multiple decomposition for identification of ED/MD resonance is also very useful[27,43]. As a result of the relatively small refractive index of $LiNbO_3$, the optical confinement inside the single nanoparticle is relatively poor, leading to relatively low electric field enhancements (with $|E|/|E_0|$ less than three, where $|E|$ is the normalized electric field intensity, and $|E_0|$ is the incident field intensity) and relatively low quality factors [with $\lambda_{res}/\Delta\lambda$ less than 20, where λ_{res} is the resonance wavelength, and $\Delta\lambda$ is the corresponding full width at half-maximum (FWHM)] for both ED and MD modes. It is worth mentioning that the optical absorption of $LiNbO_3$ at the discussed wavelength range remains extremely low and has negligible impacts on the quality factors.

3.2. Arrayed $LiNbO_3$ nanoantennas

To investigate the enhanced radiative coupling of arrayed nanoantennas based on SLRs, the $LiNbO_3$ nanoparticles (with the same geometric dimensions as those used in Section 3.1) are arranged in an infinite periodic array with square geometry. The distance between the centers of two neighboring nanoantennas represents the array's period p. By tuning the periodicity, the hybridization of Mie resonances and RAs is studied (see Fig. 3), in which both the scattering cross sections and electric field enhancements are calculated. The white lines in Fig. 3 are the lowest-order diffraction according to the RA positions:

$$\lambda_{RA} = \frac{\Lambda \cdot n_{sub}}{\sqrt{m^2 + n^2}}, \tag{1}$$

where λ_{RA} is the wavelength of the RA position (since in COMSOL simulation frequency domain is used, here the y axis in Fig. 3 uses photon energy), Λ is the period length, n_{sub} is the refractive index of the substrate (i.e., SiO_2), and m and n are integers corresponding to the diffracted order of the RAs, although only the lowest orders $(\pm 1, 0)$ and $(0, \pm 1)$ are located in the considered wavelength range. It can be found that the landscape of the ED/MD modes in a $LiNbO_3$ nanoparticle can be significantly modified by the array periodicity, resulting in RA-engineered scattering cross sections and optical field enhancements in $LiNbO_3$ nanoantennas. It is worth noting that the total induced ED/MD of an individual nanoparticle in the array is the sum of the induced ED/MD by the incident field in this nanoparticle and by the rest of the nanoparticles in the array.

With the increase of the lattice period from 900 nm to around 1425 nm, redshift and narrowing of the original MD resonances in a single nanoparticle can be observed in the arrayed nanoantennas, resulting in both scattering and electric field enhancement. The increase in the scattering cross section is due to the increased effective nanoparticle volume interacting with the light field even though the geometric cross section does not change. The highest scattering cross section and the maximum electric field enhancement [8 as illustrated in Fig. 4(a), with a quality factor close to 50] appear at periods of 1425–1450 nm. This phenomenon corresponds to a stronger coupling between single nanoparticle MD resonance and the RA [the spatial distributions of the normalized electric field intensity

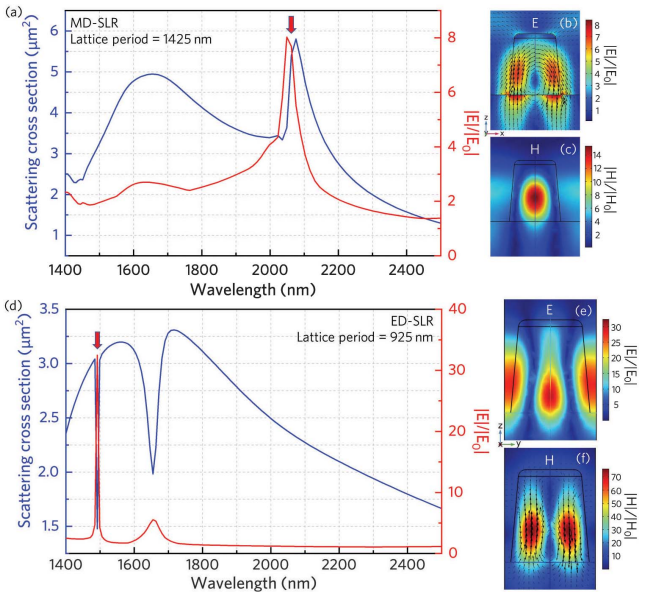

Fig. 4. COMSOL simulations of RA-engineered MD and ED modes at their maximum electric field enhancement positions (with lattice periods of 1425 nm and 925 nm). (a) Simulated scattering cross section and electric field enhancement of MD-SLR resonance and the spatial distributions of the normalized (b) electric field intensity and (c) magnetic field intensity at the maximum field enhancement position. (d) Simulated scattering cross section and electric field enhancement of ED-SLR resonance and the spatial distributions of the normalized (e) electric field intensity and (f) magnetic field intensity at the maximum field enhancement position. The color scale represents the magnetic and electric field intensity enhancements. The black arrows are the real components of the vectorial electric and magnetic fields.

and magnetic field intensity are illustrated in Figs. 4(b) and 4(c)]. The quality factor of MD-SLR is comparable to that of previously reported $LiNbO_3$ metasurfaces[27]. At the wavelength of 2076 nm (corresponding to a photon energy close to 0.60 eV), the circulation of the electric fields leads to a strong magnetic field inside the $LiNbO_3$ nanoparticle, indicating that the SLR at 2076 nm arises from the collective coupling of MD modes, which can be labeled as MD-SLR. By increasing the lattice period further from 1425 nm to 1600 nm, the coupling strength between the MD in a single nanoparticle and the RAs is weakened.

In contrast, the coupling strength between ED resonance in a single nanoparticle and the RAs is significantly enhanced by tuning the lattice period from 1600 nm to around 900 nm, resulting in a reduced scattering with a narrow spectral width with a maximum electric field enhancement of 32, which is extremely high for low-refractive-index dielectric metasurfaces. Thus, a quality factor as high as 250 at 1492 nm (corresponding to photon energy of 0.83 eV) is achieved [see Fig. 4(d)]. As suggested by the spatial distributions of the normalized electric and magnetic field intensities in Figs. 4(e) and 4(f), the strong electric field inside $LiNbO_3$ nanoparticles aligned with the incident field (x-polarized) is induced by the circulation of the magnetic fields. Therefore, the SLR formed at 1492 nm corresponds to the collective coupling of EDs in the nanoparticles, which can be labeled as ED-SLR. It is worth noting that the induced MD-SLR and ED-SLR orthogonal to each other in the nanoparticles are oriented along the direction of the incident fields.

By comparison, the field enhancement induced by ED-SLR is much higher than that of MD-SLR, partly due to the more electric intensity confined in the nanoparticle in the former case. While for MD-SLR, a large portion of the electric fields are extended outside the nanoparticles to the substrate as a result of the relatively small refractive index contrast between $LiNbO_3$ and SiO_2. Nevertheless, both of these two collective resonances show strong intensity enhancement when compared to the local fields of ED and MD resonances in a single nanoparticle, as illustrated in Fig. 2, offering a novel approach to further boost the field enhancement in $LiNbO_3$ metasurface architectures.

Considering the fabrication of $LiNbO_3$ metasurfaces, the dry etching method is one of the most commonly used methods for surface nanostructuring. However, one of the main issues of this technique on micro/nanoprocessing of $LiNbO_3$ on-chip photonic devices is the relatively large side-wall angles (i.e., θ). This factor has to be carefully considered when designing functional on-chip devices. Therefore, we further study the influence

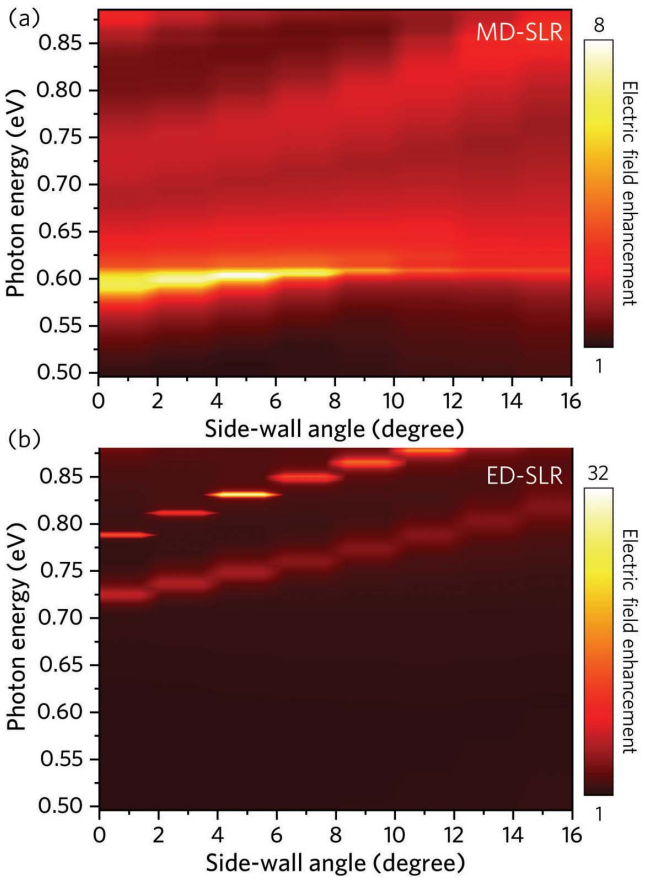

Fig. 5. COMSOL simulations of electric field enhancements of (a) MD-SLR and (b) ED-SLR in arrayed $LiNbO_3$ nanoantennas with side-wall angles tuning from 0° to 16°.

of the side-wall angle on the electric field enhancements induced by MD-SLR and ED-SLR, as illustrated in Fig. 5. For MD-SLR, by increasing the side-wall angle, the spectral width of MD-SLR narrows down and disappears when the angle is larger than 10°, indicating that the MD-SLR mode is no longer supported due to the large side-wall angle and thus the leakage of electric intensity in the nanoparticle. This is mainly because when the side-wall angle increases, the top part of the nanoparticle (with a truncated square pyramid) narrows, the optical confinement of the circular displacement current therefore weakens due to the lacking of high-refractive-index dielectrics in horizontal directions, and the electric field retardation in the nanoparticle along the propagation direction of the incident wave cannot be supported any more. While for ED-SLR, despite the reduction of the field enhancements, the ED-SLR can be still supported for large side-wall angles because, for ED resonance, no circulation of the electric field is required, relaxing the need on the nanoparticle geometry or dimensions. Moreover, blue shift of the ED-SLR resonance can be observed by increasing the side-wall angle. It is worth noting that by adjusting the nanoparticle geometry and dimension, it is still possible to further optimize the field enhancement even in case of a large side-wall angle, which has been confirmed in our simulations (not shown here).

4. Conclusions

In summary, large field enhancements and high-quality-factor resonances associated with SLRs in $LiNbO_3$ nanoantennas are numerically studied in this work, showing that the Mie resonances in a single $LiNbO_3$ nanoparticle can be significantly tailored and enhanced by collective lattice resonances, i.e., by varying the lattice period. Benefitting from the tremendous development in LNOI wafer manufacturing and high-quality $LiNbO_3$ nanofabrication technology, we envision enormous potential of high-quality-factor $LiNbO_3$ metasurfaces as resonance-enhanced linear and nonlinear components for applications in integrated nonlinear optics, including but not limited to nonlinear optical frequency converters, frequency combs, terahertz (THz) generators, etc. We should note that the lattice resonances discussed in this work can be applied for other dielectric material platforms, even materials with low refractive indices.

Acknowledgement

This work was supported by the National Key Research and Development Program of China (No. 2019YFA0705000) and Major Program of Shandong Provincial Natural Science Foundation (No. ZR2018ZB0649). Y. Jia acknowledges the support from Taishan Scholars Youth Expert Program of Shandong Province and Qilu Young Scholar Program of Shandong University, China. F. Chen thanks Taishan Scholars Climbing Program of Shandong Province for the support. The authors appreciate the valuable discussions with L. Razzari (Montréal), X. Jin (Montréal), F. Yue (Montréal), J. Dong (Montréal), and X. Wang (Shandong).

References

1. L. Novotny and N. V. Hulst, "Antennas for light," Nat. Photon. **5**, 83 (2011).
2. V. Giannini, A. I. Fern, S. C. Heck, and S. A. Maier, "Plasmonic nanoantennas: fundamentals and their use in controlling the radiative properties of nanoemitters," Chem. Rev. **111**, 3888 (2011).
3. J. N. Anker, W. P. Hall, O. Lyandres, N. C. Shah, J. Zhao, and R. P. Van Duyne, "Biosensing with plasmonic nanosensors," Nat. Mater. **7**, 442 (2008).
4. S. Hao, G. Chen, and C. Yang, "Sensing using rare-earth-doped upconversion nano-particles," Theranostics **3**, 331 (2013).
5. X. Cai, A. Lee, Z. Ji, C. Huang, C. H. Chang, X. Wang, Y. P. Liao, T. Xia, and R. Li, "Reduction of pulmonary toxicity of metal oxide nanoparticles by phosphonate-based surface passivation," Part. Fibre Toxicol. **14**, 1 (2017).
6. B. Sain, C. Meier, and T. Zentgraf, "Nonlinear optics in all-dielectric nanoantennas and metasurfaces: a review," Adv. Photon. **1**, 024002 (2019).
7. A. Krasnok, M. Tymchenko, and A. Alù, "Nonlinear metasurfaces: a paradigm shift in nonlinear optics," Mater. Today **21**, 8 (2018).
8. K. Koshelev, Y. Tang, K. Li, D.-Y. Choi, G. Li, and Y. Kivshar, "Nonlinear metasurfaces governed by bound states in the continuum," ACS Photon. **6**, 1639 (2019).
9. O. Reshef, M. Saad-Bin-Alam, M. J. Huttunen, G. Carlow, B. T. Sullivan, J.-M. Ménard, K. Dolgaleva, and R. W. Boyd, "Multiresonant high-*Q* plasmonic metasurfaces," Nano Lett. **19**, 6429 (2019).
10. M. S. Bin-Alam, O. Reshef, Y. Mamchur, M. Z. Alam, G. Carlow, J. Upham, B. T. Sullivan, J.-M. Ménard, M. J. Huttunen, R. W. Boyd, and K. Dolgaleva, "Ultra-high-*Q* resonances in plasmonic metasurfaces," Nat. Commun. **12**, 974 (2021).
11. J. Wang, A. Coillet, O. Demichel, Z. Wang, D. Rego, A. Bouhelier, P. Grelu, and B. Cluzel, "Saturable plasmonic metasurfaces for laser mode locking," Light: Sci. Appl. **9**, 50 (2020).
12. E. Rahimi and R. Gordon, "Nonlinear plasmonic metasurfaces," Adv. Opt. Mater. **6**, 1800274 (2018).
13. G. W. Castellanos, P. Bai, and J. G. Rivas, "Lattice resonances in dielectric metasurfaces," J. Appl. Phys. **125**, 213105 (2019).
14. S. Murai, G. W. Castellanos, T. V. Raziman, A. G. Curto, and J. G. Rivas, "Enhanced light emission by magnetic and electric resonances in dielectric metasurfaces," Adv. Opt. Mater. **8**, 1902024 (2020).
15. S. Lepeshov and Y. Kivshar, "Near-field coupling effects in Mie-resonant photonic structures and all-dielectric metasurfaces," ACS Photon. **5**, 2888 (2018).
16. C. Zhang, Y. Xu, J. Liu, J. Li, J. Xiang, H. Li, J. Li, Q. Dai, S. Lan, and A. E. Miroshnichenko, "Lighting up silicon nanoparticles with Mie resonances," Nat. Commun. **9**, 2964 (2018).
17. R. Weis and T. Gaylord, "Lithium niobate: summary of physical properties and crystal structure," Appl. Phys. A **37**, 191 (1985).
18. Y. Kong, F. Bo, W. Wang, D. Zheng, H. Liu, G. Zhang, R. Rupp, and J. Xu, "Recent progress in lithium niobate: optical damage, defect simulation, and on-chip devices," Adv. Mater. **32**, 1806452 (2020).
19. L. Arizmendi, "Photonic applications of lithium niobate crystals," Phys. Status Solidi A **201**, 253 (2004).
20. G. Poberaj, H. Hu, W. Sohler, and P. Günter, "Lithium niobate on insulator (LNOI) for micro-photonic devices," Laser Photon. Rev. **6**, 488 (2012).
21. A. Boes, B. Corcoran, L. Chang, J. Bowers, and A. Mitchell, "Status and potential of lithium niobate on insulator (LNOI) for photonic integrated circuits," Laser Photon. Rev. **12**, 1700256 (2018).
22. A. Honardoost, K. Abdelsalam, and S. Fathpour, "Rejuvenating a versatile photonic material: thin-film lithium niobate," Laser Photon. Rev. **14**, 2000088 (2020).
23. R. Wolf, Y. Jia, S. Bonaus, C. Werner, S. Herr, I. Breunig, K. Buse, and H. Zappe, "Quasi-phase-matched nonlinear optical frequency conversion in on-chip whispering galleries," Optica **5**, 872 (2018).
24. J. Lin, F. Bo, Y. Cheng, and J. Xu, "Advances in on-chip photonic devices based on lithium niobate on insulator," Photon. Res. **8**, 1910 (2020).
25. Y. Jia, L. Wang, and F. Chen, "Ion-cut lithium niobate on insulator technology: recent advances and perspectives," Appl. Phys. Rev. **8**, 011307 (2021).
26. B. Gao, M. Ren, W. Wu, H. Hu, W. Cai, and J. Xu, "Lithium niobate metasurfaces," Laser Photon. Rev. **13**, 1800312 (2019).
27. L. Carletti, C. Li, J. Sautter, I. Staude, C. De Angelis, T. Li, and D. N. Neshev, "Second harmonic generation in monolithic lithium niobate metasurfaces," Opt. Express **27**, 33391 (2019).

28. A. Fedotova, M. Younesi, J. Sautter, A. Vaskin, F. J. F. Löchner, M. Steinert, R. Geiss, T. Pertsch, I. Staude, and F. Setzpfandt, "Second-harmonic generation in resonant nonlinear metasurfaces based on lithium niobate," Nano Lett. **20**, 8608 (2020).
29. L. Kang, H. Bao, and D. H. Werner, "Efficient second-harmonic generation in high *Q*-factor asymmetric lithium niobate metasurfaces," Opt. Lett. **46**, 633 (2021).
30. Y. Jia, S. Wang, and F. Chen, "Femtosecond laser direct writing of flexibly configured waveguide geometries in optical crystals: fabrication and application," Opto-Electron. Adv. **3**, 190042 (2020).
31. Y. Jia and F. Chen, "Compact solid-state waveguide lasers operating in the pulsed regime: a review [Invited]," Chin. Opt. Lett. **17**, 012302 (2019).
32. Y. Niu, L. Yang, D. Guo, Y. Chen, X. Li, G. Zhao, and X. Hu, "Efficient 671 nm red light generation in annealed proton-exchanged periodically poled $LiNbO_3$ waveguides," Chin. Opt. Lett. **18**, 111902 (2020).
33. Y. Liu, X. Yan, J. Wu, B. Zhu, Y. Chen, and X. Chen, "On-chip erbium-doped lithium niobate microcavity laser," Sci. China Phys. Mech. Astron. **64**, 234262 (2021).
34. C. Zhang, Y. Lu, Y. Ni, M. Li, L. Mao, C. Liu, D. Zhang, H. Ming, and P. Wang, "Plasmonic lasing of nanocavity embedding in metallic nanoantenna array," Nano Lett. **15**, 1382 (2015).
35. A. Habib, X. Zhu, U. I. Can, M. L. McLanahan, P. Zorlutuna, and A. A. Yanik, "Electro-plasmonic nanoantenna: a nonfluorescent optical probe for ultrasensitive label-free detection of electrophysiological signals," Sci. Adv. **5**, eaav9786 (2019).
36. T. Wang, P. Li, D. N. Chigrin, A. J. Giles, F. J. Bezares, O. J. Glembocki, J. D. Caldwell, and T. Taubner, "Phonon-polaritonic bowtie nanoantennas: controlling infrared thermal radiation at the nanoscale," ACS Photon. **4**, 1753 (2017).
37. Q. Le-Van, E. Zoethout, E. J. Geluk, M. Ramezani, M. Berghuis, and J. G. Rivas, "Enhanced quality factors of surface lattice resonances in plasmonic arrays of nanoparticles," Adv. Opt. Mater. **7**, 1801451 (2019).
38. S.-D. Liu, P. Yue, S. Zhang, M. Wang, H. Dai, Y. Chen, Z.-Q. Nie, Y. Cui, J.-B. Han, and H. Duan, "Metasurfaces composed of plasmonic molecules: hybridization between parallel and orthogonal surface lattice resonances," Adv. Opt. Mater. **8**, 1901109 (2020).
39. C. Cherqui, M. R. Bourgeois, D. Wang, and G. C. Schatz, "Plasmonic surface lattice resonances: theory and computation," Acc. Chem. Res. **52**, 2548 (2019).
40. D. E. Zelmon, D. L. Small, and D. Jundt, "Infrared corrected Sellmeier coefficients for congruently grown lithium niobate and 5 mol.% magnesium oxide-doped lithium niobate," J. Opt. Soc. Am. B **14**, 3319 (1997).
41. I. H. Malitson, "Interspecimen comparison of the refractive index of fused silica," J. Opt. Soc. Am. **55**, 1205 (1965).
42. J. van de Groep and A. Polman, "Designing dielectric resonators on substrates: combining magnetic and electric resonances," Opt. Express **21**, 26285 (2013).
43. K. Jiang, Y. Wang, C. Cai, and H. Lin, "Conversion of carbon dots from fluorescence to ultralong room-temperature phosphorescence by heating for security applications," Adv. Mater. **30**, 1800783 (2018).